Wave Motion 102 (2021) 102716

Contents lists available at ScienceDirect

Wave Motion

journal homepage: www.elsevier.com/locate/wamot

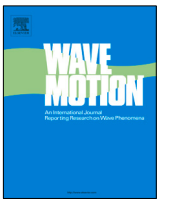

Transmission and reflection of waves at structural junctions connecting thin orthotropic plates

Nurkanat Aimakov [a,*], Gregor Tanner [a], Dimitrios Chronopoulos [b]

[a] School of Mathematical Sciences, University of Nottingham, Nottingham, NG7 2RD, UK
[b] Institute for Aerospace Technology & The Composites Group, University of Nottingham, Nottingham, NG7 2TU, UK

ARTICLE INFO

Article history:
Received 27 May 2020
Received in revised form 17 November 2020
Accepted 15 February 2021
Available online 18 February 2021

Keywords:
Structure-borne sound
Orthotropic plates
Wave scattering

ABSTRACT

We present a semi-analytical method for computing the reflection and transmission coefficients at joints connecting an arbitrary number of semi-infinite orthotropic plates based on the line-junction approximation. We use a wave approach and describe reflection, transmission and mode conversion between eigenmodes of the vibro-acoustic equations for orthotropic plates. A detailed derivation is presented here for the first time for an arbitrary number of plates meeting at the junction and without restrictions on the orientation of the principal material axes both with respect to the junction and with respect to the orientation in different plates. The approach is discussed for two specific example configurations, namely an L- and a T-shaped orthotropic plate junction. Furthermore, the scattering coefficients for a rib-stiffened orthotropic plate are derived, and the occurrence of resonance phenomena is discussed.

1. Introduction

The study of structure-borne sound propagation through plate junctions is of great importance in architectural acoustics, as well as for modelling the noise and vibration performance of mechanical structures used in transport sectors such as in the aerospace and automotive industries. Structural vibrations at low frequencies are in general modelled using deterministic schemes (e.g. the Finite Element (FE) analysis) thus capturing the full phase and amplitude information of the wave field on the structural ensemble. On the other hand, at higher frequencies, deterministic methods become inefficient and approximations based on ray- and wave-based methods or statistical approaches are favoured. For the latter type of methods, detailed information about the reflection and transmission behaviour at plate junctions is required and routinely used. Flow-balance equations such as the Statistical Energy Analysis (SEA) [1] or diffusion methods such as the Energy Flow Analysis [2] only need averaged coupling parameters, also called coupling loss factors in the context of SEA. Ray- or wave-based methods such as the Dynamical Energy Analysis (DEA) [3–5] require the full wave scattering coefficients retaining the dependence on the angle of incidence at the plate junction.

This information is usually obtained by working in the infinite junction approximation, i.e., determining the reflection and transmission coefficients by solving the wave problem for an incident plane wave assuming that the plates extend to infinity along the junction. Most of the research focused on isotropic plates so far, such as early work done by Cremer et al. [6] considering the structure-borne sound transmission of a flexural wave for right-angled joints of thin plates. Later, Craven and Gibbs [7,8] and Wöhle et al. [9,10] included the in-plane wave modes in their analyses together with considering up to four plates joined together. Langley and Heron [11] computed scattering coefficients for structural

* Corresponding author.
E-mail address: nurkanat.aimakov@nottingham.ac.uk (N. Aimakov).

https://doi.org/10.1016/j.wavemoti.2021.102716

junctions connecting an arbitrary number of thin, isotropic plates along a rigid beam. A simplified treatment using a line-junction approximation is also described in [11], that is, boundary conditions and force-balance equations are considered along a 1D line at the centre of the junction only. Mees and Vermeir [12] analysed the bending wave transmission loss in the system of plates connected by a hinge or by an elastic interlayer. McCollum and Cuschieri [13] studied the flexural behaviour of right-angled thick finite plates using a mobility power flow approach. They also considered both in-plane and out-of-plane wave scattering in right-angled thick semi-infinite plates [14]. Langley investigated wave reflection and transmission coefficients for structural junctions between curved panels and beams [15]. The occurrence of negative group velocity phenomenon in cylindrical structures has been outlined in this work. More recent works focused on wave scattering at plate junctions using hybrid FE and Wave Finite Element (WFE) [16] approaches [17–19].

Beyond the case of wave propagation in isotropic materials, Bosmans et al. [20] studied the scattering properties of orthotropic plate junctions with principal material axes aligned with the plate coordinates, that is, so-called *specially orthotropic* plates. However, no details on the derivation are given, and results are presented only for the particular case of bending wave transmission loss in right-angled plates, so-called L-junctions. It is not clear, whether the approach derived in [20] is limited to specially orthotropic plates or can be extended to an arbitrary number of plates meeting at the junction with different orientation of the principal material axes. Moreover, for a DEA treatment, detailed information on reflection/transmission behaviour of all propagating modes at complex junctions is needed. This includes information about the angle-of-incidence dependence of scattering coefficients and mode conversion factors.

We give here for the first time a detailed derivation of reflection and transmission matrices for waves travelling in structural junctions connecting two or more (thin) orthotropic plates at arbitrary angles and without any restrictions on the orientation of principal material axes both with respect to the orientation of the junction and with respect to the orientation in different plates. We discuss the method for two different junction configurations and demonstrate how the method can be used to obtain the angle-of-incidence and frequency dependence of scattering coefficients in a rib-stiffened orthotropic plate. In all calculations, we give the scattering coefficients containing the full angle-of-incidence and frequency dependence. The method has already been used to validate a WFE treatment of connected plates made of layered composite media in [21].

The manuscript is organised as follows: in Section 2, the equations for obtaining the scattering coefficients are derived in the line-junction approximation. First, the governing equations of motion for orthotropic plates are presented, and dispersion relations and group velocities for in-plane and out-of-plane waves are given. The importance of modifications to Snell's law for orthotropic plates is discussed using an example configuration. The wave dynamic stiffness matrix is then introduced, which relates displacements and forces at the junction. The individual dynamic stiffness matrices for plates are then assembled into a global equation via the application of continuity and equilibrium conditions at the junction. In Section 3, numerical case studies for two and three coupled orthotropic plates are presented. The problem of an orthotropic plate with a stiffener (of finite length) is considered as a special case; further details are presented in Appendix B. Finally, concluding remarks are given in Section 4.

2. Energy scattering coefficients for ensembles of orthotropic plates — derivation

2.1. Governing equations of motion

Consider N semi-infinite thin orthotropic plates connected along a lossless junction as shown in Fig. 1. The shared edge of the plates is aligned with the y_g axis of the global coordinate system (x_g, y_g, z_g). The position of the jth plate is described by the rotation angle ψ_j relative to the x_g axis. The position, displacements and tractions on the jth plate are defined with respect to the local coordinate system (x_j, y_j, z_j), where the local and global y axis are identical, see Fig. 2. Note that the positive direction of x_j axis always points away from the junction. We consider orthotropic plates with arbitrary principal axes, that is, the axes are not necessarily aligned with their local coordinate system.

Following Kirchhoff–Love plate theory [22,23], the governing equations of motion for the jth plate can be expressed in terms of displacements u_j, v_j, w_j as

$$\begin{aligned}
&Q_{11}\frac{\partial^2 u}{\partial x^2} + 2Q_{16}\frac{\partial^2 u}{\partial x\partial y} + Q_{66}\frac{\partial^2 u}{\partial y^2} + Q_{16}\frac{\partial^2 v}{\partial x^2} + (Q_{12}+Q_{66})\frac{\partial^2 v}{\partial x\partial y} + Q_{26}\frac{\partial^2 v}{\partial y^2} = \rho\frac{\partial^2 u}{\partial t^2},\\
&Q_{22}\frac{\partial^2 v}{\partial y^2} + 2Q_{26}\frac{\partial^2 v}{\partial x\partial y} + Q_{66}\frac{\partial^2 v}{\partial x^2} + Q_{16}\frac{\partial^2 u}{\partial x^2} + (Q_{12}+Q_{66})\frac{\partial^2 u}{\partial x\partial y} + Q_{26}\frac{\partial^2 u}{\partial y^2} = \rho\frac{\partial^2 v}{\partial t^2},\\
&D_{11}\frac{\partial^4 w}{\partial x^4} + 4D_{16}\frac{\partial^3 w}{\partial x^3\partial y} + 2(D_{12}+2D_{66})\frac{\partial^4 w}{\partial x^2\partial y^2} + 4D_{26}\frac{\partial^3 w}{\partial x\partial y^3} + D_{22}\frac{\partial^4 w}{\partial y^4} = -\rho h\frac{\partial^2 w}{\partial t^2},
\end{aligned} \tag{1}$$

where the Q_{mn}'s denote the plane stress-reduced stiffness coefficients from the constitutive relations for an orthotropic plate with $D_{mn} = Q_{mn}h^3/12$, the bending stiffnesses, ρ the material density and h the thickness. Eq. (1) are written here for the general case with principal axes not necessarily aligned with the (x, y) coordinate axes. Details about the relations between the Q_{mn}'s in Eq. (1) and the more familiar coefficients for specially orthotropic plates together with the relations to material constants can be found in Appendix A. We omit the plate index j in Eq. (1) and whenever we talk about a specific plate for ease of notation; we emphasise here that all quantities, including the material parameters, are

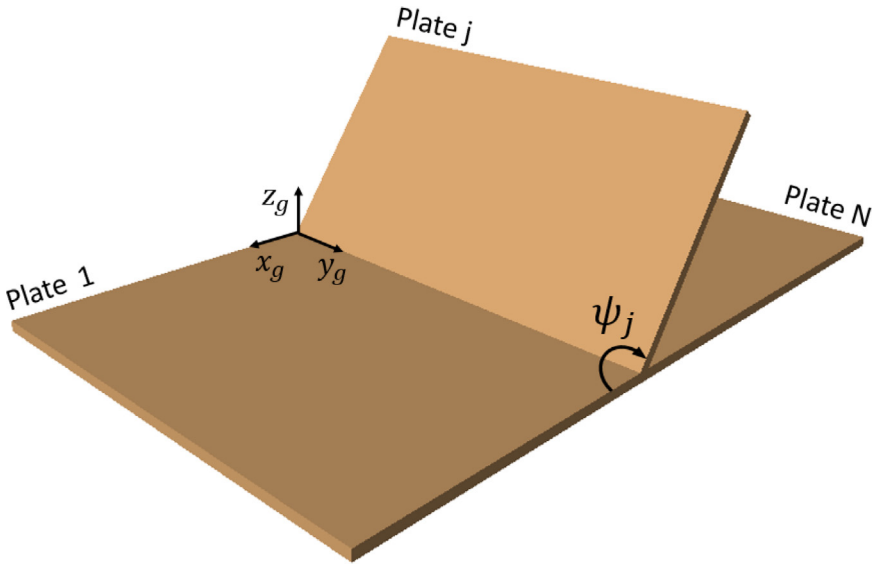

Fig. 1. The set up of N plates joined together at a common interface along the y axis.

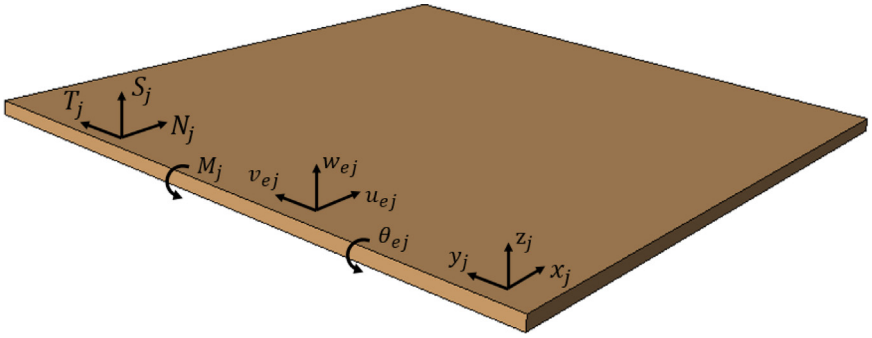

Fig. 2. Local coordinate system, displacements and tractions on the common edge "e" of the jth plate.

plate dependent. The equations of motion for in-plane and out-of-plane motion in the plate are uncoupled and so are the relations between in-plane displacements u_j, v_j to in-plane tractions N_j, T_j and out-of-plane displacement w_j and rotation θ_j to transversal traction S_j and bending moment M_j at a junction or edge "e" of that plate j, see Fig. 2. In what follows, we will use the sub-index "e", whenever we want to stress that a quantity is taken at the edge of a plate j, that is, at $x_j = 0$, following the notation in [11]. The elastic tractions can be written in the form [23]

$$\begin{aligned} N &= Q_{11}h\frac{\partial u}{\partial x} + Q_{12}h\frac{\partial v}{\partial y} + Q_{16}\,h\left(\frac{\partial u}{\partial y} + \frac{\partial v}{\partial x}\right) \\ T &= Q_{16}h\frac{\partial u}{\partial x} + Q_{26}h\frac{\partial v}{\partial y} + Q_{66}\,h\left(\frac{\partial u}{\partial y} + \frac{\partial v}{\partial x}\right) \\ S &= -D_{11}\frac{\partial^3 w}{\partial x^3} - 4D_{16}\frac{\partial^3 w}{\partial x^2\partial y} - (D_{12}+4D_{66})\,\frac{\partial^3 w}{\partial x\partial y^2} - 2D_{26}\frac{\partial^3 w}{\partial y^3} \\ M &= D_{11}\frac{\partial^2 w}{\partial x^2} + D_{12}\frac{\partial^2 w}{\partial y^2} + 2D_{16}\frac{\partial^2 w}{\partial x\partial y}\,, \end{aligned} \tag{2}$$

where we again omit the j dependence. Note that S is the Kirchhoff shear force [23,24], which includes the contribution of the twisting moment $-\frac{\partial V}{\partial y}$ together with the transversal shear traction. The twisting moment V is defined as

$$V = D_{16}\frac{\partial^2 w}{\partial x^2} + D_{26}\frac{\partial^2 w}{\partial y^2} + 2D_{66}\frac{\partial^2 w}{\partial x\partial y}\,. \tag{3}$$

It is also noted that in accordance with the plate theory used in this study, the angle of rotation θ is approximated as $\frac{\partial w}{\partial x}$.

2.2. Dispersion relations, the group velocity and Snell's law

Before discussing reflection and transmission coefficients for incoming waves at a specific angle of incidence, it is worth considering the relations between the angle of incoming and outgoing waves at an interface, that is, the relation equivalent to Snell's law for orthotropic plates.

2.2.1. Relations between incoming and outgoing waves at junctions for orthotropic plates

Since the directions of the group and phase velocities do not necessarily coincide in non-isotropic media [25], formulating the relations between the angles of incoming and outgoing waves at interfaces between plates with different material properties and thus the generalisation of Snell's law is less straightforward. The connection between group and phase velocities is provided by the dispersion relation, which needs to be studied in some detail. Given that energy is transported along the group velocity vectors, the relation between incoming and outgoing group velocity directions is essential for energy methods based on ray-tracing principals such as SEA or DEA.

Consider a plane wave of the form $e^{-\mathrm{i}k_x x-\mathrm{i}k_y y+\mathrm{i}\omega t}$ travelling across the plate, where k_x and k_y are the x and y components of the wave vector $\mathbf{k}$, and ω is the angular frequency. Substituting this plane wave solution into the 4th order bending equation (1) yields the characteristic equation for bending waves

$$D_{11}\,k_x^4 + 4D_{16}\,k_x^3\,k_y + 2(D_{12}+2D_{66})\,k_x^2\,k_y^2 + 4D_{26}\,k_x\,k_y^3 + D_{22}\,k_y^4 - \rho h\omega^2 = 0. \tag{4}$$

Following the same procedure using the first two equations in (1), the characteristic equation for in-plane waves can be expressed as

$$\begin{aligned}\left(Q_{11}\,k_x^2 + 2Q_{16}\,k_xk_y + Q_{66}\,k_y^2 - \rho\omega^2\right)\left(Q_{66}\,k_x^2 + 2Q_{26}\,k_xk_y + Q_{22}\,k_y^2 - \rho\omega^2\right) - \\ - \left(Q_{16}\,k_x^2 + (Q_{12}+Q_{66})\,k_xk_y + Q_{26}\,k_y^2\right)^2 = 0.\end{aligned} \tag{5}$$

For fixed ω, the solutions to Eqs. (4) and (5) give rise to a closed curve in (k_x, k_y) space describing the *wave vector* curves for bending, shear and longitudinal waves. We note that only real solution (k_x, k_y) describe propagating waves.

We are interested in the dynamic response of a plate j to an incident plane wave of the form $e^{\mathrm{i}k_x x-\mathrm{i}k_y y+\mathrm{i}\omega t}$ travelling towards the junction on plate j'. Compatibility conditions at the junction yield the response of the plate j in the form $e^{-\mathrm{i}\mu x-\mathrm{i}k_y y+\mathrm{i}\omega t}$, that is, k_y and ω are *common to all plates on the edge "*e*"*. The x component of the wave vector, here denoted μ, is then computed from the dispersion relations in Eqs. (4) and (5). For the out-of-plane motion, one obtains four solutions of Eq. (4) which come in pairs of roots $\mu^{\pm}$. One pair is either real or complex corresponding to propagating or attenuating bending waves, respectively. We denote this pair as $\mu^{\pm}_{B_1}$ where the superscripts " + " and " − " represent outgoing and incoming waves. The other pair of roots denoted $\mu^{\pm}_{B_2}$ is always complex; the corresponding bending waves are thus attenuating.

Similarly, the dispersion relations (5) can be solved for the unknown μ yielding a characteristic equation with four roots $\mu^{\pm}_{L,S}$ that represent real or complex incoming and outgoing quasi-longitudinal and quasi-shear waves, here denoted as L and S, respectively. Valid plate responses, that is, outgoing waves with μ^{+}_{X}, $X = B_1, B_2, L$ and S either oscillate with a positive energy flux along the x axis or attenuate exponentially with increasing x, see Section 2.3.1 for more details. In the example to follow below, we will only consider the propagating branches and explain the relation between the directions of incoming and outgoing waves, which follows from the continuity condition $k_y = const$.

For this, we also need the group velocity vector $\mathbf{c}_g$, which gives the direction of the wave energy flow [26]. The standard definition $\mathbf{c}_g = \partial\omega/\partial\mathbf{k}$ is not convenient for our purposes here, since the dependence of the angular frequency ω on the wave vector $\mathbf{k}$ is only implicitly given through the dispersion relations (4) and (5). Instead, one can use

$$\left(c_{gx}, c_{gy}\right) = -\frac{1}{\dfrac{\partial\Omega}{\partial\omega}}\left(\frac{\partial\Omega}{\partial k_x}, \frac{\partial\Omega}{\partial k_y}\right) \tag{6}$$

to find the components of the group velocities c_{gx} and c_{gy} [26] for different modes. Here, $\Omega = \Omega\left(k_x, k_y, \omega\right)$ is the left hand side of either the dispersion relations (4) or (5).

2.2.2. Snell's law for orthotropic plates — an example

We will discuss some of the peculiarities of the interplay between incoming and outgoing wave directions at interfaces between orthotropic plates by looking at a specific example. We consider here two identical orthotropic plates meeting at an angle ψ as shown in Fig. 1, but with principal material axes rotated against each other. The actual value of ψ is not essential for the discussion in this section; it will be set to $\psi = 90°$ when reconsidering this example in Section 3.1. The material characteristics of the plates are given as: $h = 0.005\,\mathrm{m}$, $E_x = 121\,\mathrm{GPa}$, $E_y = 8.6\,\mathrm{GPa}$, $G_{xy} = 4.7\,\mathrm{GPa}$, $\nu_{xy} = 0.27$ and $\rho = 1490\,\mathrm{kg/m^3}$; for the relations connecting these material parameters to the stiffness coefficients in Eq. (1), see Appendix A. We work at a frequency of 3000 Hz here, a frequency value consistent with the thin plate assumptions for the parameters chosen. The orientation of the principal material axes of the two plates with respect to the interface and with respect to each other is important; here, we chose the angle of rotation of the material axes in each plate to be 45° with respect to the local coordinate system as defined in Fig. 2, see also Fig. 6 for the $\psi = 90°$ example discussed

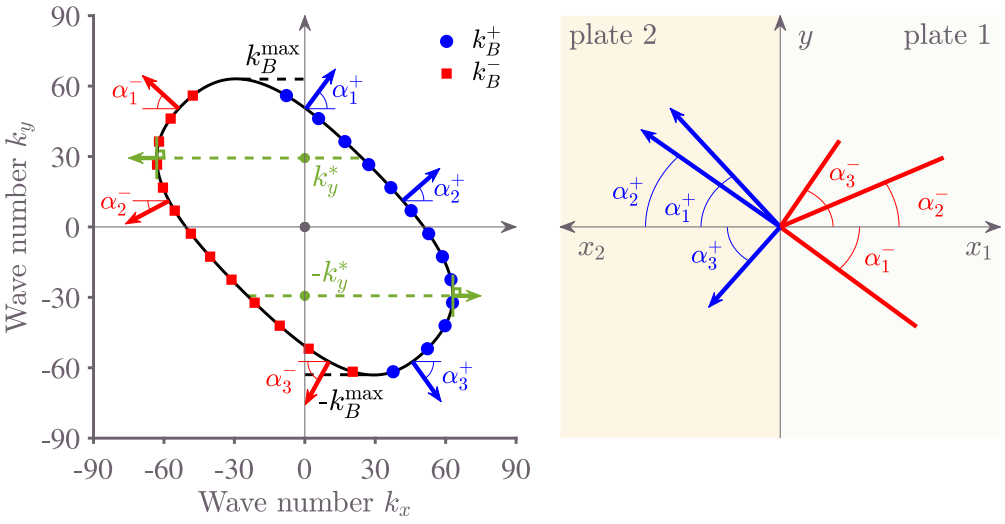

Fig. 3. Bending wave vector curve in a 45° rotated orthotropic plate at a frequency 3000 Hz (left) and a schematic representation of incoming/outgoing waves at the junction of two identical plates (right). Blue dots represent wave numbers related to outgoing waves while red squares correspond to incoming waves. Wave number components $k_B^{\max}$ and k_y^* equal to $62.96\,\mathrm{m}^{-1}$ and $29.34\,\mathrm{m}^{-1}$, respectively.

in Section 3.1. The left-hand side of Fig. 3 shows the bending wave vector curve at a frequency 3000 Hz obtained from Eq. (4) in the local coordinate system displaying the 45° rotation. Note that the wave vector curve is the same for both plates in their local coordinate system. The range of k_y values which allow for propagating bending waves at 3000 Hz is between $(-k_B^{\max}, k_B^{\max})$. We emphasise again that the angle ψ between the two plates can take arbitrary values here; for the sake of clarity, we have drawn the local coordinates of the plates, (x_i, y) with $i = 1$ or 2, in the same plane on the right-hand side of Fig. 3 and in Fig. 4 below.

As we are interested in the energy flow across interfaces, the relevant angles of incidence, reflection and transmission are those obtained from the group velocity vectors, Eq. (6); they point along the gradient vectors to the wave vector curves (denoted by the angles $\alpha_j^{\pm}$ in Fig. 3). Here, blue symbols correspond to velocity vectors with a positive x component describing waves transporting energy away from the junction, and red symbols describe incoming energy fluxes. The continuity condition $k_y = const$ now connects incoming with outgoing group velocity directions on the wave vector curve, that is, red squares (incoming) with blue dots (outgoing). This leads to a peculiar effect here: in the range $k_y^* < |k_y| < k_B^{\max}$, propagating waves, for example with angles of incidence $\alpha_{1,3}^-$, are transmitted or reflected keeping their direction of travel in the y direction, see the right side of Fig. 3. This is what one usually finds at refracting interfaces. However, for $-k_y^* < k_y < k_y^*$, a wave, for example with incident angle α_2^-, is scattered reversing its direction in the y-direction, see α_2^+ in Fig. 3. This gives rise to negative refraction for these values of k_y. The phenomenon is displayed in more detail in Fig. 4 representing group velocity rays transmitting from one plate to another; the region in blue shows the negative refraction phenomenon.

Furthermore, note that the group velocity vector α_3^- points in the opposite x direction compared to the corresponding wave vector, see Fig. 3. This implies that the individual wavefronts travel away from junction whereas the wave energy travels towards it. Similar behaviour can be encountered for wave vectors in the upper part of the dispersion curve; for specific values of $k_y > k_y^*$ the outgoing wavefronts travel towards the junction whereas the wave energy propagates away from it.

Interesting features can also be seen for in-plane wave vector curves, as shown in Fig. 5. The shape of the longitudinal wave vector curve is similar to that of the bending wave. Therefore it also exhibits negative refraction and opposition of phase and group velocity vector directions for specific fixed values of k_y. The shear wave vector curve shows additional features due to its peculiar form, which we cannot discuss here in all details. We just mention that there exists a set of values of k_y (labelled $k_{S_2}^*$ in Fig. 5), for which there are two pairs of incoming and outgoing shear waves for each k_y. Finally, propagating longitudinal and shear waves can only exist for k_y values in the range $(-k_L^{\max}, k_L^{\max})$ and $(-k_S^{\max}, k_S^{\max})$, respectively. Beyond these intervals, the corresponding propagating waves become attenuating. We will come back to this example in Section 3.1.

2.3. Derivation of the dynamic stiffness matrix

Next, we are interested in the local dynamic stiffness matrix for the plate j. This matrix relates boundary forces to boundary displacements produced by the waves emerging from a junction in the form $e^{-\mathrm{i}\mu x - \mathrm{i}k_y y + \mathrm{i}\omega t}$. As discussed in Section 2.2.1, k_y and ω are common to all plates meeting at an edge "e" and the x components of the wave vectors, μ,

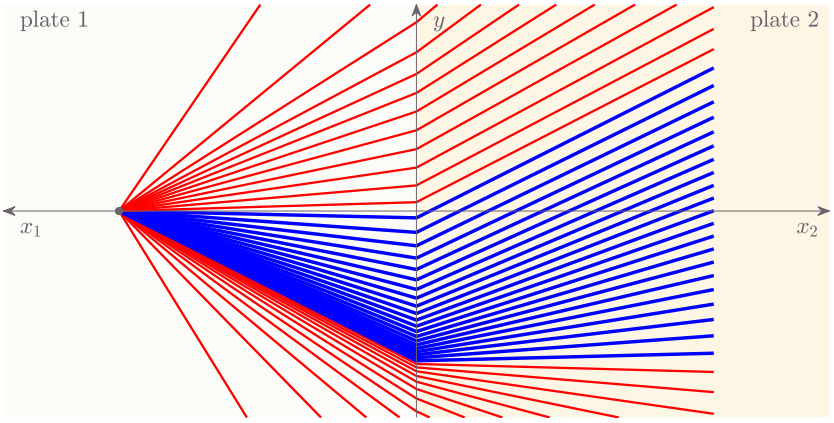

Fig. 4. Group velocity ray picture for bending waves at junction of two identical 45° rotated orthotropic plates at a frequency 3000 Hz. Blue lines highlight the region of incoming rays, which represents the negative refractive index phenomenon. (For interpretation of the references to colour in this figure legend, the reader is referred to the web version of this article.)

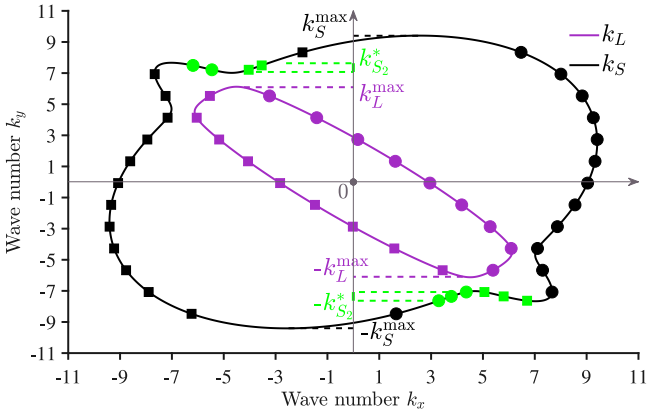

Fig. 5. Longitudinal and shear wave vector curves in a 45° rotated orthotropic plate at a frequency 3000 Hz. Dots represent wave numbers related to outgoing waves while squares – incoming waves. Wave number components k_L^* and k_S^* equal to $6\,\mathrm{m}^{-1}$ and $9.3\,\mathrm{m}^{-1}$, respectively – the critical values for longitudinal and shear waves.

are obtained from the dispersion relations (4) and (5) with solutions forming real or complex pairs $\mu_X^{\pm}$ with $X = B_1, B_2, L$ or S.

2.3.1. Energy flow and the response of the plate

The bending wave energy flow in the x direction can be generally written as [27]

$$J_B = \frac{1}{2}\,\mathrm{Re}\left(\mathrm{i}\omega \begin{bmatrix} w & \theta & \frac{\partial w}{\partial y} \end{bmatrix}^* \begin{bmatrix} S + \frac{\partial V}{\partial y} \\ M \\ V \end{bmatrix}\right), \tag{7}$$

where * denotes complex conjugation and $\theta = \frac{\partial w}{\partial x}$ as mentioned in Section 2.1. Now, introducing $w = e^{-\mathrm{i}\mu_B x - \mathrm{i}k_y y + \mathrm{i}\omega t}$ into Eq. (7) yields

$$J_{B_{1,2}}^{\pm} = \frac{1}{2}\,\mathrm{Re}\left(\mathrm{i}\omega \begin{bmatrix} 1 & -\mathrm{i}\mu_{B_{1,2}}^{\pm} & -\mathrm{i}k_y \end{bmatrix}^* \begin{bmatrix} S_{1,2}^{\pm} + \frac{\partial V_{1,2}^{\pm}}{\partial y} \\ M_{1,2}^{\pm} \\ V_{1,2}^{\pm} \end{bmatrix}\right). \tag{8}$$

Furthermore, $S_{1,2}^{\pm}$, $M_{1,2}^{\pm}$ and $V_{1,2}^{\pm}$ are given by Eqs. (2) and (3) with $\frac{\partial}{\partial x}$ and $\frac{\partial}{\partial y}$ replaced by $-\mathrm{i}\mu_{B_{1,2}}^{\pm}$ and $-\mathrm{i}k_y$, respectively.

As mentioned in Section 2.2.1, propagating incoming or outgoing waves are those with real wave number components $\mu_{B_1}^{\pm}$ giving rise to an energy flux to or away from the junction, that is, $J_{B_1}^{\pm} < 0$ or $J_{B_1}^{\pm} > 0$, respectively. If the $\mu_{B_{1,2}}^{\pm}$ are complex with $\mathrm{Re}\left(\mu_{B_{1,2}}^{\pm}\right) \neq 0$, then the outgoing or incoming waves oscillate while decaying or increasing exponentially

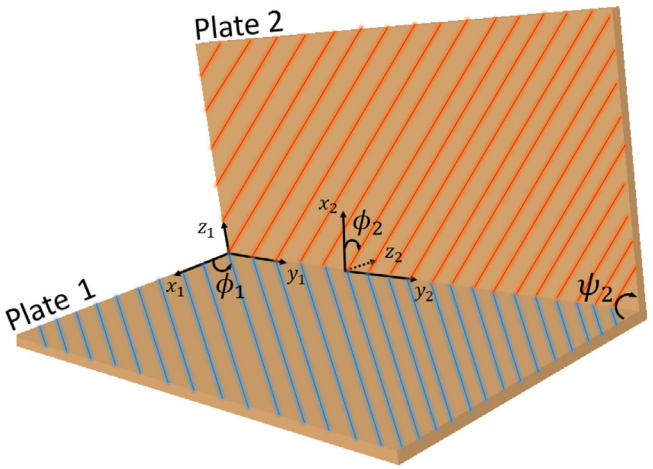

Fig. 6. Schematic of an L-junction. The angle ψ_2 here is set to 90°. Red and blue lines represent the fibre direction of the plates. The local angles of orientations ϕ_1 and ϕ_2 are both set to 45°. (For interpretation of the references to colour in this figure legend, the reader is referred to the web version of this article.)

along the x axis. This leads to energy transport as well, that is, the energy flux $J^{\pm}_{B_{1,2}} \neq 0$. This phenomenon is caused by the fact that the direction of the decaying/increasing wave is not aligned with the x direction [28,29]. Consequently, a wave shape projection along the x axis can appear to be oscillating, (see for example Fig. 8 in [28]).

Once the appropriate bending wave number roots $\mu^{+}_{B_{1,2}}$ are defined, the out-of-plane response of the plate can be expressed as

$$w^{+} = \alpha^{+}_{B_1} e^{-\mathrm{i}\mu^{+}_{B_1} x - \mathrm{i}k_y y + \mathrm{i}\omega t} + \alpha^{+}_{B_2} e^{-\mathrm{i}\mu^{+}_{B_2} x - \mathrm{i}k_y y + \mathrm{i}\omega t}, \tag{9}$$

where the constants $\alpha^{+}_{B_1}$ and $\alpha^{+}_{B_2}$ are amplitudes of the outgoing bending waves.

For the in-plane motion, the response of the plate takes the form

$$\begin{aligned} u &= \Phi_u e^{-\mathrm{i}\mu x - \mathrm{i}k_y y + \mathrm{i}\omega t}, \\ v &= \Phi_v e^{-\mathrm{i}\mu x - \mathrm{i}k_y y + \mathrm{i}\omega t}. \end{aligned} \tag{10}$$

The dispersion relations (5) can be solved for the unknown μ yielding a characteristic equation with four roots $\mu^{\pm}_{L,S}$ that represent incoming and outgoing quasi-longitudinal and quasi-shear waves, here denoted again as L and S, respectively. Similar to the out-of-plane case, a valid outgoing solution produces a positive energy flow in the x direction if the correspondent wave is propagating, or it is associated with complex-valued $\mu^{+}_{L,S}$ with $\mathrm{Im}(\mu^{+}_{L,S}) < 0$, that is, the correspondent wave is exponentially attenuating as $x \to \infty$. Note that purely imaginary solutions of Eq. (5) $\mu^{+}_{L,S}$, which are present in specially orthotropic plates, produce no energy flow since the corresponding waves are evanescent.

The energy flow in the x direction of in-plane waves can be generally written as

$$J = \frac{1}{2}\,\mathrm{Re}\left(\mathrm{i}\omega \begin{bmatrix} u & v \end{bmatrix}^{*} \begin{bmatrix} N \\ T \end{bmatrix}\right). \tag{11}$$

Introducing Eqs. (10) into Eq. (11) yields the energy flow expressions for the longitudinal and shear wave modes, that is,

$$J^{\pm}_{L} = \frac{1}{2}\,\mathrm{Re}\left(\mathrm{i}\omega \begin{bmatrix} 1 & \Phi^{\pm}_{L} \end{bmatrix}^{*} \begin{bmatrix} N^{\pm}_{L} \\ T^{\pm}_{L} \end{bmatrix}\right) \quad , \quad J^{\pm}_{S} = \frac{1}{2}\,\mathrm{Re}\left(\mathrm{i}\omega \begin{bmatrix} \Phi^{\pm}_{S} & 1 \end{bmatrix}^{*} \begin{bmatrix} N^{\pm}_{S} \\ T^{\pm}_{S} \end{bmatrix}\right), \tag{12}$$

with

$$\Phi^{\pm}_{L} = \frac{Q_{16}\,\mu^{\pm 2}_{L} + k_y\,\mu^{\pm}_{L}\,(Q_{12}+Q_{66}) + Q_{26}k_y^2}{-Q_{66}\,\mu^{\pm 2}_{L} - 2\,Q_{26}\,k_y\,\mu^{\pm}_{L} - Q_{22}k_y^2 + \rho\omega^2} \quad , \quad \Phi^{\pm}_{S} = \frac{Q_{16}\,\mu^{\pm 2}_{S} + k_y\,\mu^{\pm}_{S}\,(Q_{12}+Q_{66}) + Q_{26}k_y^2}{-Q_{11}\,\mu^{\pm 2}_{S} - 2\,Q_{16}\,k_y\,\mu^{\pm}_{S} - Q_{66}k_y^2 + \rho\omega^2}, \tag{13}$$

where $\begin{bmatrix} 1 & \Phi^{\pm}_{L} \end{bmatrix}^{T}$ and $\begin{bmatrix} \Phi^{\pm}_{S} & 1 \end{bmatrix}^{T}$ are the eigenvectors in the Φ_u, Φ_v basis corresponding to the wave numbers $\mu^{\pm}_{L}$ and $\mu^{\pm}_{S}$ for incoming and outgoing modes. $N^{\pm}_{L,S}$ and $T^{\pm}_{L,S}$ are given by substituting $\frac{\partial}{\partial x}$ and $\frac{\partial}{\partial y}$ by $-\mathrm{i}\mu^{\pm}_{L,S}$ and $-\mathrm{i}k_y$ in Eqs. (2), respectively.

The in-plane response of the plate can be written as

$$\begin{bmatrix} u^{+} \\ v^{+} \end{bmatrix} = \alpha^{+}_{L} \begin{bmatrix} 1 \\ \Phi^{+}_{L} \end{bmatrix} e^{-\mathrm{i}\mu^{+}_{L} x - \mathrm{i}k_y y + \mathrm{i}\omega t} + \alpha^{+}_{S} \begin{bmatrix} \Phi^{+}_{S} \\ 1 \end{bmatrix} e^{-\mathrm{i}\mu^{+}_{S} x - \mathrm{i}k_y y + \mathrm{i}\omega t}, \tag{14}$$

where α_L^+ and α_S^+ are the amplitudes of outgoing quasi-longitudinal and quasi-shear waves. This particular choice of eigenvectors ensures the correct representation of the displacement field in the case of $k_y = 0$ and $Q_{16} = Q_{26} = 0$, that is, when the incident plane wave vector is directed normal to the junction and the plate is specially orthotropic. Then $\Phi_L^+ = \Phi_S^+ = 0$, and the response of the plate can be expressed as

$$\begin{aligned} u^+ &= \alpha_L^+ e^{-\mathrm{i}\tilde{\mu}_L^+ x + \mathrm{i}\omega t} \\ v^+ &= \alpha_S^+ e^{-\mathrm{i}\tilde{\mu}_S^+ x + \mathrm{i}\omega t}. \end{aligned} \tag{15}$$

The values $\tilde{\mu}_L^+ = \sqrt{\rho\omega^2/Q_{11}}$ and $\tilde{\mu}_S^+ = \sqrt{\rho\omega^2/Q_{66}}$ agree then with the wave numbers of purely longitudinal and shear waves, respectively, and the in-plane response of the plate consists of purely longitudinal and shear displacements in the x and y directions.

2.3.2. The dynamic stiffness matrix

As described in Section 2.3, we are interested in the local dynamic stiffness matrix of the semi-infinite plate j that relates boundary forces with boundary displacements produced by plane waves of the form $e^{-\mathrm{i}\mu x - \mathrm{i}k_y y + \mathrm{i}\omega t}$. Using Eq. (9), one can define the out-of-plane displacement w^+ and rotation θ^+ at the common intersection "e" at $x = 0$ in terms of the amplitudes $\alpha_{B_1}^+$ and $\alpha_{B_2}^+$, that is,

$$\begin{bmatrix} w_{\mathrm{e}}^+ \\ \theta_{\mathrm{e}}^+ \end{bmatrix} = \begin{bmatrix} 1 & 1 \\ -\mathrm{i}\mu_{B_1}^+ & -\mathrm{i}\mu_{B_2}^+ \end{bmatrix} \begin{bmatrix} \alpha_{B_1}^+ \\ \alpha_{B_2}^+ \end{bmatrix} e^{-\mathrm{i}k_y y + \mathrm{i}\omega t}. \tag{16}$$

The elastic tractions involving the out-of-plane displacement can be written in terms of the same amplitudes $\alpha_{B_1}^+$ and $\alpha_{B_2}^+$ by inserting Eq. (9) in Eqs. (2), that is,

$$\begin{aligned} S_{\mathrm{e}}^+ &= \sum_{m=1}^{2} \left(D_{11}\,\mathrm{i}\mu_{B_m}^{+3} - 4D_{16}\,\mu_{B_m}^{+2}\,\mathrm{i}k_y - (D_{12} + 4D_{66})\,\mathrm{i}\mu_{B_m}^+ k_y^2 - 2D_{26}\,\mathrm{i}k_y^3 \right) \alpha_{B_m}^+ e^{-\mathrm{i}k_y y + \mathrm{i}\omega t}, \\ M_{\mathrm{e}}^+ &= \sum_{m=1}^{2} \left(-D_{11}\,\mu_{B_m}^{+2} - D_{12}\,k_y^2 - 2D_{16}\,\mu_{B_m}^+ k_y \right) \alpha_{B_m}^+ e^{-\mathrm{i}k_y y + \mathrm{i}\omega t}. \end{aligned} \tag{17}$$

Finally, combining Eq. (16) with Eqs. (17) yields a relation between the elastic tractions S_{e}^+, M_{e}^+ and the edge displacement w_{e}^+ and rotation θ_{e}^+ at $x = 0$, that is,

$$\begin{bmatrix} S_{\mathrm{e}}^+ \\ M_{\mathrm{e}}^+ \end{bmatrix} = \begin{bmatrix} -D_{11}\,\mathrm{i}\mu_{B_1}^+\mu_{B_2}^+\left(\mu_{B_1}^+ + \mu_{B_2}^+\right) + 4D_{16}\,\mu_{B_1}^+\mu_{B_2}^+\,\mathrm{i}k_y - 2D_{26}\,\mathrm{i}k_y^3 & D_{11}\,\mu_{B_1}^+\mu_{B_2}^+ - D_{12}k_y^2 \\ -D_{11}\left(\mu_{B_1}^{+2} + \mu_{B_2}^{+2} + \mu_{B_1}^+\mu_{B_2}^+\right) + 4D_{16}\left(\mu_{B_1}^+ + \mu_{B_2}^+\right)k_y + (D_{12} + 4D_{66})\,k_y^2 & -D_{11}\mathrm{i}\left(\mu_{B_1}^+ + \mu_{B_2}^+\right) - 2D_{16}\mathrm{i}k_y \end{bmatrix}^T \begin{bmatrix} w_{\mathrm{e}}^+ \\ \theta_{\mathrm{e}}^+ \end{bmatrix}. \tag{18}$$

Eq. (18) describes the part of the dynamic stiffness matrix for out-of-plane displacement w_{e}^+ and rotation θ_{e}^+.

Next, we consider the corresponding part for in-plane motion. The in-plane displacements u_{e}^+ and v_{e}^+ at the shared edge are given as

$$\begin{bmatrix} u_{\mathrm{e}}^+ \\ v_{\mathrm{e}}^+ \end{bmatrix} = \begin{bmatrix} 1 & \Phi_S^+ \\ \Phi_L^+ & 1 \end{bmatrix} \begin{bmatrix} \alpha_L^+ \\ \alpha_S^+ \end{bmatrix} e^{-\mathrm{i}k_y y + \mathrm{i}\omega t}. \tag{19}$$

Now, inserting Eq. (14) into Eqs. (2) yields a relation between the in-plane tractions and the amplitudes of the outgoing in-plane waves, that is,

$$\begin{bmatrix} N_{\mathrm{e}}^+ \\ T_{\mathrm{e}}^+ \end{bmatrix} = -\mathrm{i}h \begin{bmatrix} Q_{11}\mu_L^+ + Q_{12}\Phi_L^+ k_y + Q_{16}\left(\Phi_L^+\mu_L^+ + k_y\right) & Q_{11}\Phi_S^+\mu_S^+ + Q_{12}k_y + Q_{16}\left(\mu_S^+ + \Phi_S^+ k_y\right) \\ Q_{16}\mu_L^+ + Q_{26}\Phi_L^+ k_y + Q_{66}\left(\Phi_L^+\mu_L^+ + k_y\right) & Q_{16}\Phi_S^+\mu_S^+ + Q_{26}k_y + Q_{66}\left(\mu_S^+ + \Phi_S^+ k_y\right) \end{bmatrix} \begin{bmatrix} \alpha_L^+ \\ \alpha_S^+ \end{bmatrix} e^{-\mathrm{i}k_y y + \mathrm{i}\omega t}. \tag{20}$$

Eliminating α_L^+ and α_S^+ in Eq. (20) using Eq. (19) gives

$$\begin{bmatrix} N_{\mathrm{e}}^+ \\ T_{\mathrm{e}}^+ \end{bmatrix} = -\mathrm{i}h \begin{bmatrix} cQ_{11}\left(\mu_L^+ - \Phi_L^+\Phi_S^+\mu_S^+\right) + Q_{16}\left(c\Phi_L^+\left(\mu_L^+ - \mu_S^+\right) + k_y\right) & cQ_{16}\left(\mu_S^+ - \Phi_L^+\Phi_S^+\mu_L^+\right) + cQ_{11}\Phi_S^+\left(\mu_S^+ - \mu_L^+\right) + Q_{12}k_y \\ cQ_{16}\left(\mu_L^+ - \Phi_L^+\Phi_S^+\mu_S^+\right) + Q_{66}\left(c\Phi_L^+\left(\mu_L^+ - \mu_S^+\right) + k_y\right) & cQ_{66}\left(\mu_S^+ - \Phi_L^+\Phi_S^+\mu_L^+\right) + cQ_{16}\Phi_S^+\left(\mu_S^+ - \mu_L^+\right) + Q_{26}k_y \end{bmatrix} \begin{bmatrix} u_{\mathrm{e}}^+ \\ v_{\mathrm{e}}^+ \end{bmatrix}, \tag{21}$$

where $c = \dfrac{1}{1 - \Phi_L^+\Phi_S^+}$. The matrix in Eq. (21) is the part of the dynamic stiffness matrix related to in-plane motion.

We now define the elastic tractions and displacements at the junction edge as $F = (N_{\mathrm{e}}, T_{\mathrm{e}}, S_{\mathrm{e}}, M_{\mathrm{e}})^T$ and $U = (u_{\mathrm{e}}, v_{\mathrm{e}}, w_{\mathrm{e}}, \theta_{\mathrm{e}})^T$ and write

$$F_j^+ = K_j^+ U_j^+ \tag{22}$$

for the relation between the displacements of an outgoing wave at the edge of plate j and the associate forces, where the 4×4 dynamic stiffness matrix K_j^+ is a block matrix defined through Eqs. (18) and (21). An associated stiffness matrix K_j^- relating displacements of the incoming waves U_j^- with forces F_j^- can be obtained from K_j^+ by changing the corresponding wave number components μ^+ by μ^- in the sub-matrices related to in-plane and out-of-plane motion. In what follows, it will also be important to consider the relation between displacements and mode amplitudes. We denote $A^\pm = \left(\alpha_L^\pm, \alpha_S^\pm, \alpha_{B_1}^\pm, \alpha_{B_2}^\pm\right)^T$ as the vector of amplitudes of incoming or outgoing modes, and write

$$U_j^\pm = H_j^\pm A_j^\pm \tag{23}$$

on the edge of plate j, where $H_j^\pm$ is the block-diagonal matrix obtained from Eqs. (16) and (19). Here, H_j^- is obtained from H_j^+ by changing the wave number components μ^+ by μ^-. In the next step, we will derive the global dynamic stiffness matrices of each plate junction and associated scattering matrices using force equilibrium conditions and continuity conditions at the junction.

2.4. Reflection and transmission at plate junctions

Assuming no external forces are applied at the junction, one can write the force equilibrium and continuity conditions at an edge shared between N plates as

$$\sum_{j=1}^{N} R_j F_j = 0, \tag{24}$$

$$U_j = R_j^T U \quad \text{for all } j = 1, \ldots, N, \tag{25}$$

where $F_j = F_j^+ + F_j^-$ and $U_j = U_j^+ + U_j^-$ is the total force and displacement at the edge of plate j. U denotes the displacement common to all plates (continuity) and R_j is the rotation matrix from the local coordinate system $\left(x_j, y_j, z_j\right)$ to the global coordinate system $\left(x_g, y_g, z_g\right)$, that is,

$$R_j = \begin{bmatrix} \cos\psi_j & 0 & -\sin\psi_j & 0 \\ 0 & 1 & 0 & 0 \\ \sin\psi_j & 0 & \cos\psi_j & 0 \\ 0 & 0 & 0 & 1 \end{bmatrix}. \tag{26}$$

Rewriting Eq. (24) using Eq. (22), we obtain

$$\sum_{j=1}^{N} R_j K_j^+ U_j^+ = -\sum_{j=1}^{N} R_j K_j^- U_j^- \tag{27}$$

$$\Rightarrow \sum_{j=1}^{N} R_j K_j^+ U_j = \sum_{j=1}^{N} R_j \left(K_j^+ - K_j^-\right) U_j^-. \tag{28}$$

Using Eq. (25), we can now deduce the common displacement vector U as a function of the incoming waves, that is,

$$U = \left(\sum_{j=1}^{N} R_j K_j^+ R_j^T\right)^{-1} \sum_{n=1}^{N} R_n \left(K_n^+ - K_n^-\right) U_n^-. \tag{29}$$

Inserting Eq. (29) into the N matrix Eqs. (25), one obtains for $m = 1, \ldots, N$

$$U_m^+ = R_m^T \left(\sum_{j=1}^{N} R_j K_j^+ R_j^T\right)^{-1} \left(\sum_{n=1}^{N} R_n \left(K_n^+ - K_n^-\right) U_n^-\right) - U_m^-, \tag{30}$$

and writing this in terms of the mode amplitudes using Eq. (23), we obtain

$$A_m^+ = \left(H_m^+\right)^{-1} R_m^T \left(\sum_{j=1}^{N} R_j K_j^+ R_j^T\right)^{-1} \left(\sum_{n=1}^{N} R_n \left(K_n^+ - K_n^-\right) H_n^- A_n^-\right) - \left(H_m^+\right)^{-1} H_m^- A_m^-. \tag{31}$$

Eq. (31) gives relations between incoming and outgoing wave mode amplitudes and can be interpreted as defining the matrix elements of a $4N \times 4N$ scattering matrix S. We are in general interested in the energy scattering coefficients, that is, the ratio between outgoing and incident energy fluxes. Writing the matrix elements of S in the form $s_{ij}^{nm}\left(\omega, k_y\right)$ for an

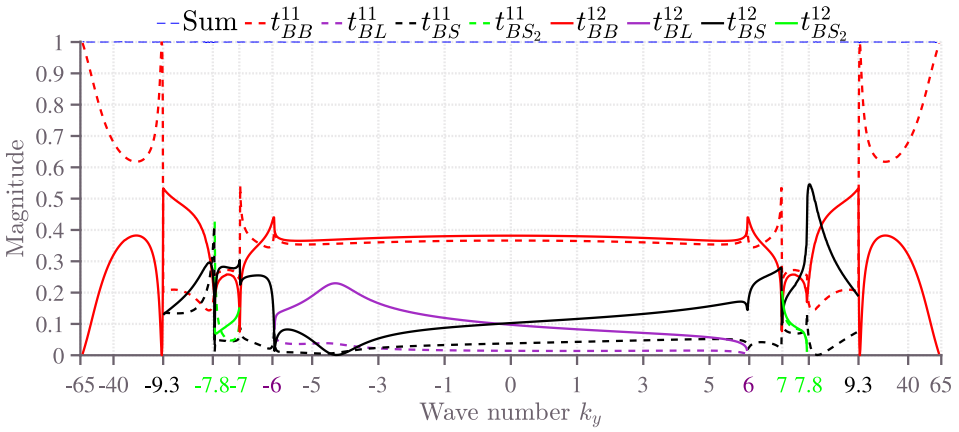

(a) Incoming bending wave B

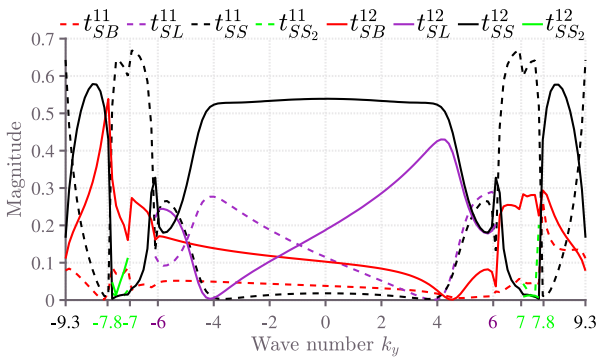

(b) Incoming shear wave S

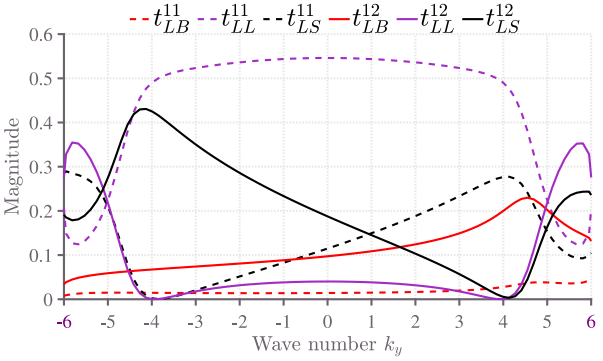

(c) Incoming longitudinal wave L

Fig. 7. Energy scattering coefficients of an L-joint for various incident waves as a function of wave number component k_y at a frequency 3000 Hz. (For interpretation of the references to colour in this figure legend, the reader is referred to the web version of this article.)

incoming wave of type i in plate n and a reflected or transmitted wave of type j in plate m (at angular frequency ω and wave number component k_y), we obtain for the associated energy fluxes

$$t_{ij}^{nm}\left(\omega, k_y\right) = \begin{cases} \dfrac{J^{+}_{j,m}}{J^{-}_{i,n}} |s_{ij}^{nm}|^2 & \text{if wave } j \text{ is propagating.} \\ 0 & \text{otherwise.} \end{cases} \tag{32}$$

Here, $J^{-}_{i,n}$ ($J^{+}_{j,m}$) is the incoming (outgoing) energy flux of type i (j) on plate n (m) given by either Eq. (12) for in-plane modes or Eq. (8) for out-of-plane motion. It is noted here that the sum of energy scattering coefficients over the outgoing modes equals one, that is,

$$\sum_{m=1}^{N} \sum_{j} t_{ij}^{nm} = 1 \tag{33}$$

due to energy conservation. We will use this relation as a check in the examples below.

3. Computational results

In the following, we will consider some particular examples in more detail, consisting of orthotropic plates joined together in the form of L and T junctions. Only the scattering coefficients for the propagating waves will be shown, and we denote the bending waves as B (instead of B_1) for simplicity. The evanescent contributions are of course considered in full in the actual computations.

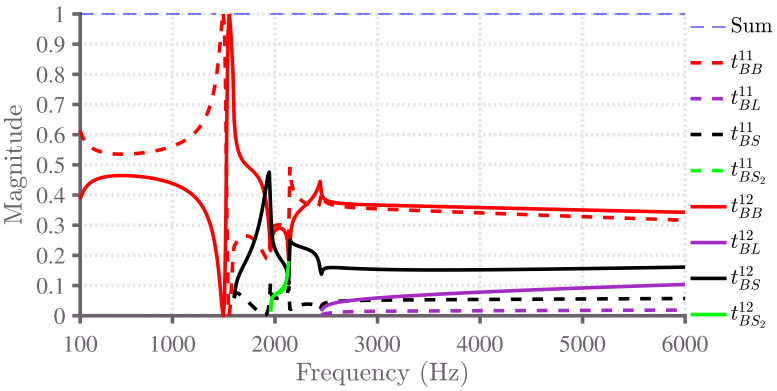

Fig. 8. Energy scattering coefficients of an L-joint for an incident bending wave as a function of frequency for a wave number component $k_y = 5\,\mathrm{m}^{-1}$.

3.1. Two orthotropic plates joined at a right angle

We first go back to the example considered in Section 2.2.2, that is, two identical orthotropic plates with principal material axes rotated by 45° with respect to the local coordinate systems, that is, $\phi_1 = \phi_2 = 45°$ in Fig. 6. We fix the inter-plate angle to $\psi = 90°$, that is, the plate configuration has the form of an L-junction. Fig. 7 shows the energy scattering coefficients for this L-junction for incident bending, shear or longitudinal modes as a function of the wave number component k_y at 3000 Hz. Note, that reflection and transmission coefficients of bending, shear and longitudinal waves without mode conversion (having the form t^{ij}_{XX} with $X = B, L, S$ and $i, j = 1, 2$) are symmetric around $k_y = 0$ whereas coefficients describing scattering between different modes, that is, $t^{ij}_{XX'}$ with $X \neq X'$ are non-symmetric. The phenomenon of mode conversion is observed only between certain critical values: for an incoming bending mode, these are the k_y values between $\pm 9.3\,\mathrm{m}^{-1}$ for reflected or transmitted shear waves and $\pm 6\,\mathrm{m}^{-1}$ for longitudinal waves. Furthermore, for $7\,\mathrm{m}^{-1} \leq |k_y| \leq 7.8\,\mathrm{m}^{-1}$, mode conversion to the second shear wave (labelled S_2) can occur. For example, the incoming shear wave power P with $k_y \sim 7.2\,\mathrm{m}^{-1}$ is reflected back with $0.6P$, converted to the second shear wave with $0.1P$ and reflected/transmitted as a bending wave, both with $0.1P$, see Fig. 7(b). These critical values of k_y can be determined from the dispersion relations (4) and (5) and correspond to the wave numbers $k_L^{\max}$, $k_S^{\max}$ and $k_{S_2}^*$ shown in Fig. 5.

Note that the energy scattering coefficients sum up to one according to Eq. (33) which is used here as a check of consistency of the results (dashed blue line in Fig. 7(a), not shown in the other sub-figures). If the wave number component k_y is fixed, and the frequency is varied instead, one can find critical frequencies at which mode conversion phenomena start to occur. For example, in the case of an incident bending wave with $k_y = 5m^{-1}$, outgoing shear waves become propagating at $f \geq 1601$ Hz, whereas outgoing longitudinal waves become propagating for $f \geq 2453$ Hz, see Fig. 8. Mode conversion from incident bending wave to the second shear wave S_2 occurs in the frequency range $f \in [1956, 2133]$ Hz.

3.2. Stiffened orthotropic plates

In this example, we consider an orthotropic plate with a stiffener, that is, an infinite orthotropic plate together with an orthotropic plate of finite length fixed at 90°, see Fig. 9. The intersection (or common edge) has thus the form of a T-junction with angles $\psi_1 = 0°$, $\psi_2 = 180°$ and $\psi_3 = 90°$. All material properties of the plates are the same as in the case of the L-junction. The local angles of orientation of principal material axes are $\phi_1 = 45°$, $\phi_2 = -45°$ and $\phi_3 = 45°$, where ϕ_2 is given a value of $-45°$ to ensure that plates 1 and 2 form a uniform ground plate. The length of the third plate is denoted as l, and the ground plate is assumed to be infinite in both x directions. We are interested, how the energy flux generated by an incident wave in the ground plate is partitioned between reflected and transmitted outgoing energy fluxes again in the ground plate. Since the third plate is of finite length, waves being transmitted into the stiffener reflect at the free boundary and become incident on the junction again leading to further reflection, transmission and mode conversion. This leads to resonance effects. Our description in terms of local scattering matrices relating incoming to outgoing modes at junctions as derived in Section 2 provides an ideal framework to handle such multi-reflection and transmission phenomena. Details of the derivation are referred to Appendix B.

In Fig. 10, we display the energy scattering coefficients as a function of the wave number component k_y for a stiffener of length $l = 30$ cm with an incident bending wave at frequency 3000 Hz. Critical angles for longitudinal and shear waves remain the same as discussed in the previous section and only bending waves can propagate for $|k_y| > 9.3\,\mathrm{m}^{-1}$. One observes resonant behaviour of the reflected and transmitted energy flux coefficients t^{11}_{BB} and t^{12}_{BB} at certain k_y values, which can be related to the resonance condition (B.10). At resonance, an incoming wave is either totally transmitted or reflected, see Fig. 10.

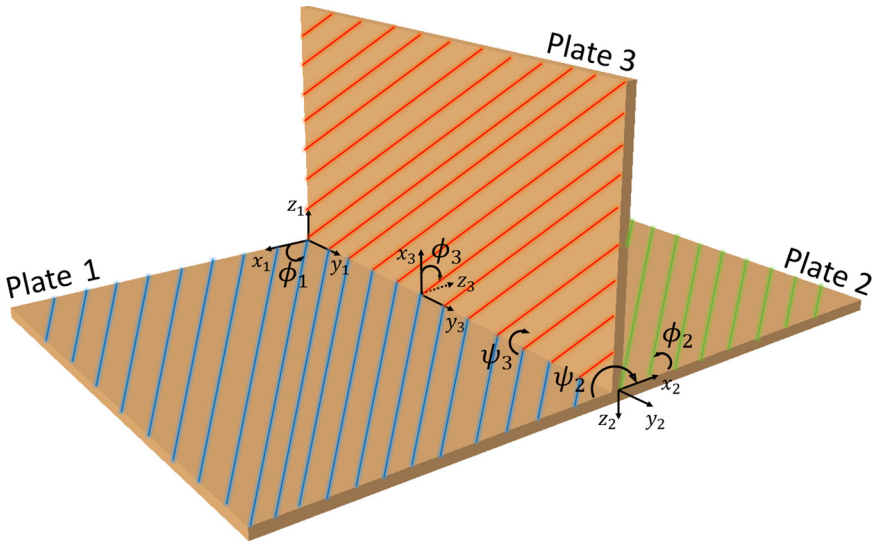

Fig. 9. Schematic of the stiffened plate. The angles ψ_2 and ψ_3 here are set to 180° and 90°, respectively. Red, blue and green lines represent the fibre direction of the plates. The local angles of orientations ϕ_1 and ϕ_3 are both set to 45°, whereas ϕ_2 is equal to −45°. (For interpretation of the references to colour in this figure legend, the reader is referred to the web version of this article.)

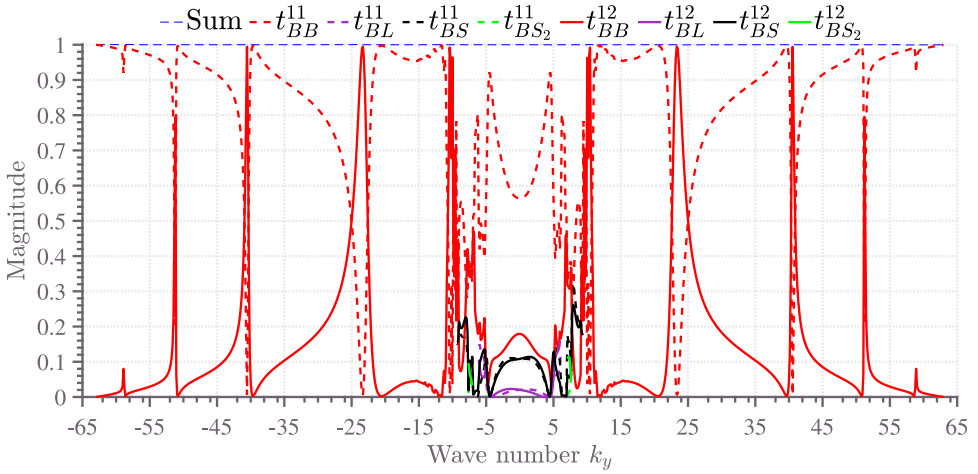

Fig. 10. Energy scattering coefficients of a stiffened plate for an incident bending wave as a function of wave number component k_y at a frequency 3000 Hz.

A similar phenomenon can be observed for the case of fixed wave number component k_y and varying frequency. Fig. 11 presents the frequency dependency of the energy scattering coefficients for $k_y = 0$, that is, for the case of normal incidence of the wave vector **k**. Several things are noted here. Firstly, at $k_y = 0$ mode conversion is possible at all frequencies and significant coupling between modes is present near resonance frequencies, such as 2600 Hz and 3900 Hz. Secondly, at resonance frequencies, especially in the band [100−2000] Hz, bending waves behave similarly as in the case of varying k_y, that is, waves are mainly reflected or transmitted except for some coupling to shear and longitudinal waves. The energy scattering coefficients sum up to one in the absence of damping as expected.

4. Conclusion

The paper describes in all generality, how to compute energy scattering coefficients of structural junctions made up of thin orthotropic plates in the line junction approximation. Expressions quantifying transmission and reflection coefficients as a function of the frequency and the wave number component k_y have been derived. Interesting phenomena such as negative refraction and negative group velocity have been observed and analysed. The scattering coefficients have been computed explicitly for examples consisting of two and three orthotropic plates joined together in an L and T geometry.

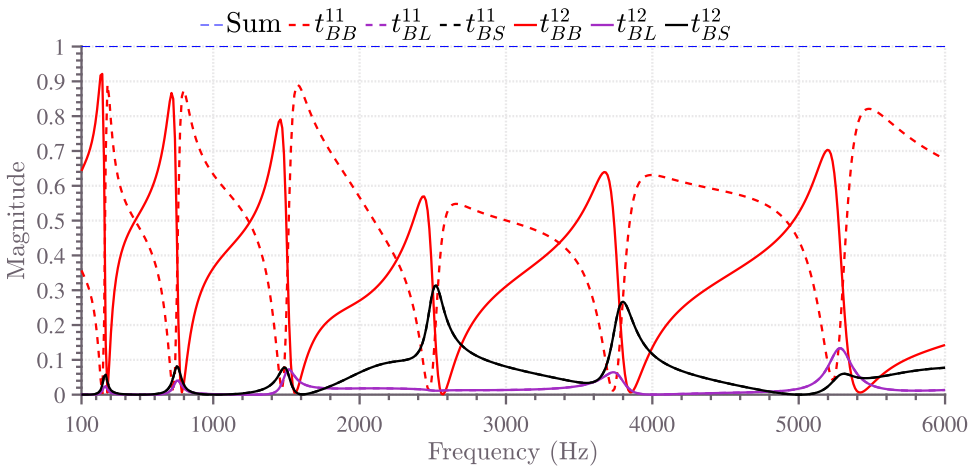

Fig. 11. Energy scattering coefficients of a stiffened plate for an incident bending wave as a function of frequency at a wave number component $k_y = 0$.

The special case of a stiffened orthotropic plate has been considered. The method gives for the first time a detailed recipe for computing scattering coefficients for the generic case of an arbitrary number of orthotropic plates connected at a junction without restrictions on the angles at which the plate meet or the orientation of the principal axis of individual plates. This information is of importance for energy flow methods such as SEA or DEA. A detailed comparison with a numerically exact computation going beyond the line junction approximation based on the Wave Finite Element Method has been partly presented in [21].

CRediT authorship contribution statement

Nurkanat Aimakov: Conceptualization, Methodology, Software, Validation, Writing - original draft, Writing - review & editing, Visualisation. **Gregor Tanner:** Conceptualization, Writing - review & editing, Supervision. **Dimitrios Chronopoulos:** Conceptualization, Writing - review & editing, Supervision.

Declaration of competing interest

The authors declare that they have no known competing financial interests or personal relationships that could have appeared to influence the work reported in this paper.

Acknowledgements

This work has been undertaken as part of the INNOVATIVE doctoral training programme, partially funded by the Marie Curie Initial Training Networks (ITN), EU action (project number 665468) and partially by the Institute for Aerospace Technology, UK (IAT) at the University of Nottingham.

Appendix A. Plane stress-reduced stiffnesses

The plane stress-reduced stiffnesses Q_{ij} of a generally orthotropic plate in Eqs. (1) can be related to the stiffness coefficients $\bar{Q}_{ij}$ of the same plate described in a local coordinate system aligned with the principal material coordinate axes as follows:

$$\begin{aligned}
Q_{11} &= \bar{Q}_{11}\cos^4\phi + 2\left(\bar{Q}_{12}+2\bar{Q}_{66}\right)\sin^2\phi\cos^2\phi + \bar{Q}_{22}\sin^4\phi,\\
Q_{12} &= \left(\bar{Q}_{11}+\bar{Q}_{22}-4\bar{Q}_{66}\right)\sin^2\phi\cos^2\phi + \bar{Q}_{12}\left(\sin^4\phi+\cos^4\phi\right),\\
Q_{22} &= \bar{Q}_{11}\sin^4\phi + 2\left(\bar{Q}_{12}+2\bar{Q}_{66}\right)\sin^2\phi\cos^2\phi + \bar{Q}_{22}\sin^4\phi,\\
Q_{16} &= \left(\bar{Q}_{11}-\bar{Q}_{12}-2\bar{Q}_{66}\right)\sin\phi\cos^3\phi + \left(\bar{Q}_{12}-\bar{Q}_{22}+2\bar{Q}_{66}\right)\sin^3\phi\cos\phi,\\
Q_{26} &= \left(\bar{Q}_{11}-\bar{Q}_{12}-2\bar{Q}_{66}\right)\sin^3\phi\cos\phi + \left(\bar{Q}_{12}-\bar{Q}_{22}+2\bar{Q}_{66}\right)\sin\phi\cos^3\phi,\\
Q_{66} &= \left(\bar{Q}_{11}+\bar{Q}_{22}-2\bar{Q}_{12}-2\bar{Q}_{66}\right)\sin^2\phi\cos^2\phi + \bar{Q}_{66}\left(\sin^4\phi+\cos^4\phi\right).
\end{aligned} \tag{A.1}$$

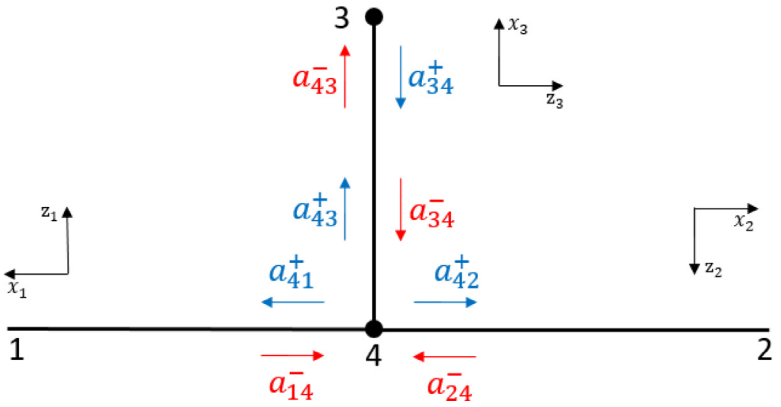

Fig. B1. A schematic view of a stiffened plate in the xz plane. Here, a_{ij}^{-} represent the amplitudes of incoming waves, and a_{ij}^{+}, the amplitudes of outgoing waves.

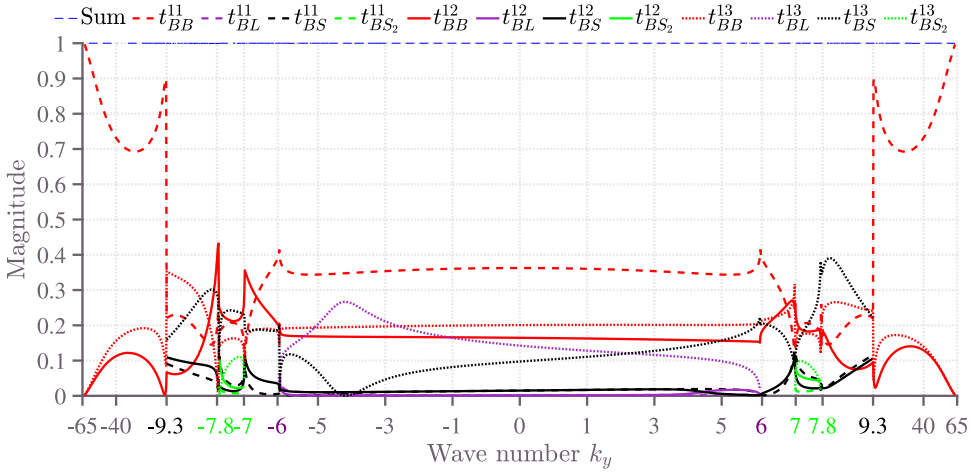

Fig. B2. Energy scattering coefficients of a T-joint for an incident bending wave as a function of wave number component k_y at a frequency 3000 Hz.

Here, ϕ is the angle of rotation of the principal material coordinate system with respect to the local coordinate system of the plate. Furthermore, $\bar{Q}_{ij}$ can be expressed in terms of the material constants as follows:

$$\bar{Q}_{11} = \frac{E_x}{1-\nu_{xy}\nu_{yx}}, \quad \bar{Q}_{22} = \frac{E_y}{1-\nu_{xy}\nu_{yx}}, \quad \bar{Q}_{12} = \nu_{xy}\bar{Q}_{22}, \quad \bar{Q}_{66} = G_{xy}, \quad \nu_{yx} = \nu_{xy}\frac{E_y}{E_x}. \tag{A.2}$$

Note, that for $\phi = \pi n/2, n \in \mathbb{Z}$, the plane stress-reduced stiffnesses Q_{16} and Q_{26} are equal to zero, the corresponding plates are called *specially orthotropic*.

Appendix B. Stiffened plate

We give here the details for computing the scattering coefficients for a plate with a stiffener attached, as shown in Fig. 9. We are interested in the reflection and transmission coefficients between points 1 and 2 in Fig. B1 taking into account that the excitation can also enter the stiffener at point 4 and being reflected at the free end at point 3. In order to compute the energy scattering coefficients in Eq. (32) relating plate one and two, one needs to compute the associate scattering matrix s_{eff} from the scattering matrix at junction 4, but including waves travelling into the stiffener and being reflected at the end of the stiffener at 3. Fig. B2 presents the energy scattering coefficients for an incoming bending wave at junction 4 in the case of semi-infinite T-plate, that is, without including the contribution of waves that being reflected at point 3.

Following the treatment in [30] extended to the elastodynamic case in [31], we now introduce the amplitudes of incoming and outgoing waves at each of the plate segments shown in Fig. B1, that is,

$$a_{ij}^{\pm} = \begin{bmatrix} a_L^{\pm} \\ a_S^{\pm} \\ a_{B_1}^{\pm} \\ a_{B_2}^{\pm} \end{bmatrix}_{ij} \qquad i,j \in (1,2,3,4)\,, \tag{B.1}$$

where the subscript ij is related to a wave travelling from i to j as shown in Fig. B1. Following this notation, we write the two scattering matrices at the junction 4 and free edge 3 obtained from Eq. (31) as

$$\begin{bmatrix} a_{41}^{+} \\ a_{42}^{+} \\ a_{43}^{+} \end{bmatrix} = S^{(4)} \begin{bmatrix} a_{14}^{-} \\ a_{24}^{-} \\ a_{34}^{-} \end{bmatrix} = \begin{bmatrix} \rho_{11} & \tau_{21} & \tau_{31} \\ \tau_{12} & \rho_{22} & \tau_{32} \\ \tau_{13} & \tau_{23} & \rho_{33} \end{bmatrix} \begin{bmatrix} a_{14}^{-} \\ a_{24}^{-} \\ a_{34}^{-} \end{bmatrix}, \quad a_{34}^{+} = S^{(3)} a_{43}^{-} = \tilde{\rho}_{33} a_{43}^{-}\,, \tag{B.2}$$

where the sub-matrices in (B.2) contain the scattering coefficients s_{ij}^{nm} from plate n to m of mode type i to j in the form

$$\rho_{nn} = \begin{bmatrix} s_{LL}^{nn} & s_{LS}^{nn} & s_{B_1L}^{nn} & s_{B_2L}^{nn} \\ s_{LS}^{nn} & s_{SS}^{nn} & s_{B_1S}^{nn} & s_{B_2S}^{nn} \\ s_{LB_1}^{nn} & s_{SB_1}^{nn} & s_{B_1B_1}^{nn} & s_{B_2B_1}^{nn} \\ s_{LB_2}^{nn} & s_{SB_2}^{nn} & s_{B_1B_2}^{nn} & s_{B_2B_2}^{nn} \end{bmatrix}, \qquad \tau_{nm} = \begin{bmatrix} s_{LL}^{nm} & s_{LS}^{nm} & s_{B_1L}^{nm} & s_{B_2L}^{nm} \\ s_{LS}^{nm} & s_{SS}^{nm} & s_{B_1S}^{nm} & s_{B_2S}^{nm} \\ s_{LB_1}^{nm} & s_{SB_1}^{nm} & s_{B_1B_1}^{nm} & s_{B_2B_1}^{nm} \\ s_{LB_2}^{nm} & s_{SB_2}^{nm} & s_{B_1B_2}^{nm} & s_{B_2B_2}^{nm} \end{bmatrix}. \tag{B.3}$$

Note that $\tilde{\rho}_{33}$ denotes the reflection matrix at node 3 and is different from ρ_{33} corresponding to reflection of waves on node 4 incoming from plate 3. The amplitudes a_{43}^{+} of outgoing waves are related to the amplitudes a_{43}^{-} of the incoming waves, that is,

$$a_{43}^{-} = \mathrm{P}\, a_{43}^{+} \quad , \quad \mathrm{P} = \mathrm{diag}\left(e^{-\mathrm{i}\mu^{+}l}\right), \tag{B.4}$$

where $\mu^{+} = \begin{bmatrix} \mu_L^{+} & \mu_S^{+} & \mu_{B_1}^{+} & \mu_{B_2}^{+} \end{bmatrix}^T$ and $\mathrm{diag}\left(e^{-\mathrm{i}\mu^{+}l}\right)$ represents the diagonal matrix with $\exp(-\mathrm{i}\mu^{+}l)$ on its diagonal (see [30,31]). The same applies for the pair of amplitudes of outgoing and incoming waves a_{34}^{+} and a_{34}^{-}, that is,

$$a_{34}^{-} = \tilde{\mathrm{P}}\, a_{34}^{+} \quad , \quad \tilde{\mathrm{P}} = \mathrm{diag}\left(e^{-\mathrm{i}\tilde{\mu}^{+}l}\right). \tag{B.5}$$

Note that $\tilde{\mu}^{+}$ are computed in the local coordinate system of semi-infinite plate with the free edge. Its principal material axes must be rotated to $-\phi_3$ to ensure that waves with amplitudes $a_{43(34)}^{-}$ and $a_{43(34)}^{+}$ have the same angle of propagation. This entails $\tilde{\mu}^{+} \neq \mu^{+}$ for $\phi_3 \neq 0°$ or $\pm 90°$, and consequently, $\tilde{\mathrm{P}} \neq \mathrm{P}$ for such cases. Now, by eliminating a_{43}^{+} and a_{34}^{-} in (B.2), one can derive the effective scattering matrix which links amplitudes of outgoing waves a_{41}^{+} and a_{42}^{+} with incoming waves a_{14}^{-} and a_{24}^{-}. Considering, for example, the third row of the matrix equation in (B.2), that is,

$$a_{43}^{+} = \tau_{13} a_{14}^{-} + \tau_{23} a_{24}^{-} + \rho_{33} a_{34}^{-}. \tag{B.6}$$

By using (B.4), (B.5) and the second equation in (B.2), one obtains

$$a_{34}^{-} = \tilde{\mathrm{P}}\, \tilde{\rho}_{33} \mathrm{P}\, a_{43}^{+}, \tag{B.7}$$

which combined with (B.6) and (B.7) yields the following matrix equation for a_{34}^{-}:

$$\left(\mathrm{I} - \tilde{\mathrm{P}}\, \tilde{\rho}_{33} \mathrm{P}\, \rho_{33}\right) a_{34}^{-} = \tilde{\mathrm{P}}\, \tilde{\rho}_{33} \mathrm{P} \left(\tau_{13} a_{14}^{-} + \tau_{23} a_{24}^{-}\right). \tag{B.8}$$

Finally, the effective scattering matrix s_{eff} is obtained as

$$s_{eff} = \begin{bmatrix} \rho_{11} + \tau_{31} \left(\mathrm{I} - \tilde{\mathrm{P}}\, \tilde{\rho}_{33} \mathrm{P}\, \rho_{33}\right)^{-1} \tilde{\mathrm{P}}\, \tilde{\rho}_{33} \mathrm{P}\, \tau_{13} & \tau_{21} + \tau_{31} \left(\mathrm{I} - \tilde{\mathrm{P}}\, \tilde{\rho}_{33} \mathrm{P}\, \rho_{33}\right)^{-1} \tilde{\mathrm{P}}\, \tilde{\rho}_{33} \mathrm{P}\, \tau_{23} \\ \tau_{12} + \tau_{32} \left(\mathrm{I} - \tilde{\mathrm{P}}\, \tilde{\rho}_{33} \mathrm{P}\, \rho_{33}\right)^{-1} \tilde{\mathrm{P}}\, \tilde{\rho}_{33} \mathrm{P}\, \tau_{13} & \rho_{22} + \tau_{32} \left(\mathrm{I} - \tilde{\mathrm{P}}\, \tilde{\rho}_{33} \mathrm{P}\, \rho_{33}\right)^{-1} \tilde{\mathrm{P}}\, \tilde{\rho}_{33} \mathrm{P}\, \tau_{23} \end{bmatrix}. \tag{B.9}$$

The effective energy scattering coefficients t_{ij}^{nm}, $n, m \in \{1, 2\}$ can be computed from s_{eff} using Eq. (32). Note that $\tilde{\mathrm{P}}\, \tilde{\rho}_{33} \mathrm{P}\, \rho_{33}$ is sub-unitary due to the sub-unitarity of ρ_{33}, and s_{eff} in (B.9) is thus not singular.

A resonance condition can be formulated, that is, resonances are attained at wave numbers k_y and frequencies ω values giving rise to local minima of

$$\left|\det\left(\mathrm{I} - \tilde{\mathrm{P}}\, \tilde{\rho}_{33} \mathrm{P}\, \rho_{33}\right)\right|. \tag{B.10}$$

References

[1] R.H. Lyon, R.G. DeJong, M. Heckl, Theory and Application of Statistical Energy Analysis, Elsevier, 1995, http://dx.doi.org/10.1016/C2009-0-26747-X.
[2] P. Cho, R. Bernhard, Energy flow analysis of coupled beams, J. Sound Vib. 211 (4) (1998) 593–605, http://dx.doi.org/10.1006/jsvi.1997.1350.
[3] G. Tanner, Dynamical energy analysis—Determining wave energy distributions in vibro-acoustical structures in the high-frequency regime, J. Sound Vib. 320 (4–5) (2009) 1023–1038, http://dx.doi.org/10.1016/j.jsv.2008.08.032.
[4] D. Chappell, D. Löchel, N. Søndergaard, G. Tanner, Dynamical energy analysis on mesh grids: A new tool for describing the vibro-acoustic response of complex mechanical structures, Wave Motion 51 (4) (2014) 589–597, http://dx.doi.org/10.1016/j.wavemoti.2014.01.004.
[5] T. Hartmann, S. Morita, G. Tanner, D.J. Chappell, High-frequency structure- and air-borne sound transmission for a tractor model using Dynamical Energy Analysis, Wave Motion 87 (2019) 132–150, http://dx.doi.org/10.1016/j.wavemoti.2018.09.012.
[6] L. Cremer, M. Heckl, Structure-Borne sound, in: Struct. Sound, Springer-Verlag, 1973, http://dx.doi.org/10.1007/978-3-662-10118-6.
[7] P.G. Craven, B.M. Gibbs, Sound transmission and mode coupling at junctions of thin plates, part I: Representation of the problem, J. Sound Vib. 77 (3) (1981) 417–427, http://dx.doi.org/10.1016/S0022-460X(81)80177-0.
[8] B.M. Gibbs, P.G. Craven, Sound transmission and mode coupling at junctions of thin plates, part II: Parametric survey, J. Sound Vib. 77 (3) (1981) 429–435, http://dx.doi.org/10.1016/S0022-460X(81)80178-2.
[9] W. Wöhle, T. Beckmann, H. Schreckenbach, Coupling loss factors for statistical energy analysis of sound transmission at rectangular structural slab joints, part I, J. Sound Vib. 77 (3) (1981) 323–334, http://dx.doi.org/10.1016/S0022-460X(81)80169-1.
[10] W. Wöhle, T. Beckmann, H. Schreckenbach, Coupling loss factors for statistical energy analysis of sound transmission at rectangular structural slab joints, part II, J. Sound Vib. 77 (3) (1981) 335–344, http://dx.doi.org/10.1016/S0022-460X(81)80170-8.
[11] R.S. Langley, K.H. Heron, Elastic wave transmission through plate/beam junctions, J. Sound Vib. 143 (2) (1990) 241–253, http://dx.doi.org/10.1016/0022-460X(90)90953-W.
[12] P. Mees, G. Vermeir, Structure-borne sound transmission at elastically connected plates, J. Sound Vib. 166 (1) (1993) 55–76, http://dx.doi.org/10.1006/jsvi.1993.1283.
[13] M.D. McCollum, J.M. Cuschieri, Thick plate bending wave transmission using a mobility power flow approach, J. Acoust. Soc. Am. 88 (3) (1990) 1472–1479, http://dx.doi.org/10.1121/1.400303.
[14] M.D. McCollum, J.M. Cuschieri, Bending and in-plane wave transmission in thick connected plates using statistical energy analysis, J. Acoust. Soc. Am. 88 (3) (1990) 1480–1485, http://dx.doi.org/10.1121/1.400304.
[15] R. Langley, Elastic wave transmission coefficients and coupling loss factors for structural junctions between curved panels, J. Sound Vib. 169 (3) (1994) 297–317, http://dx.doi.org/10.1006/jsvi.1994.1020.
[16] D. Mead, A general theory of harmonic wave propagation in linear periodic systems with multiple coupling, J. Sound Vib. 27 (2) (1973) 235–260, http://dx.doi.org/10.1016/0022-460X(73)90064-3.
[17] J.M. Mencik, M.N. Ichchou, Multi-mode propagation and diffusion in structures through finite elements, Eur. J. Mech. A Solids 24 (5) (2005) 877–898, http://dx.doi.org/10.1016/j.euromechsol.2005.05.004.
[18] J.M. Renno, B.R. Mace, Calculation of reflection and transmission coefficients of joints using a hybrid finite element/wave and finite element approach, J. Sound Vib. 332 (9) (2013) 2149–2164, http://dx.doi.org/10.1016/j.jsv.2012.04.029.
[19] G. Mitrou, N. Ferguson, J. Renno, Wave transmission through two-dimensional structures by the hybrid FE/WFE approach, J. Sound Vib. 389 (2017) 484–501, http://dx.doi.org/10.1016/j.jsv.2016.09.032.
[20] I. Bosmans, P. Mees, G. Vermeir, Structure-borne sound transmission between thin orthotropic plates: analytical solutions, J. Sound Vib. 191 (1) (1996) 75–90, http://dx.doi.org/10.1006/jsvi.1996.0107.
[21] N. Aimakov, G. Tanner, D. Chronopoulos, Wave scattering in coupled composite plates, in: INTER-NOISE NOISE-CON Congr. Conf. Proc., Institute of Noise Control Engineering, Ibiza, 2018, pp. 421–431.
[22] A. Love, On the small free vibrations and deformations of thin elastic shells, Philos. Trans. R. Soc. (1888).
[23] J.E. Ashton, J.M. Whitney, Theory of Laminated Plates, Technomic, 1970.
[24] A. Le Bot, Foundation of Statistical Energy Analysis in Vibroacoustics, Oxford University Press, 2015, p. 400, http://dx.doi.org/10.1093/acprof:oso/9780198729235.001.0001.
[25] K.F. Graff, Wave Motion in Elastic Solids, Clarendon Press, Oxford, 1975.
[26] B. Auld, Acoustic Fields and Waves in Solids, John Wiley & Sons, 1973.
[27] X. Pan, C.H. Hansen, Active control of vibratory power transmission along a semi-infinite plate, J. Sound Vib. 184 (4) (1995) 585–610, http://dx.doi.org/10.1006/jsvi.1995.0335.
[28] I. Thompson, I.D. Abrahams, A.N. Norris, On the existence of flexural edge waves on thin orthotropic plates, J. Acoust. Soc. Am. 112 (5) (2002) 1756–1765, http://dx.doi.org/10.1121/1.1506686.
[29] D.D. Zakharov, Konenkov's waves in anisotropic layered plates, Acoust. Phys. 48 (2) (2002) 171–175, http://dx.doi.org/10.1134/1.1460953.
[30] T. Kottos, U. Smilansky, Quantum chaos on graphs, Phys. Rev. Lett. 79 (24) (1997) 4794–4797, http://dx.doi.org/10.1103/PhysRevLett.79.4794.
[31] C. Brewer, S.C. Creagh, G. Tanner, Elastodynamics on graphs—wave propagation on networks of plates, J. Phys. A Math. Theor. 51 (44) (2018) 445101, http://dx.doi.org/10.1088/1751-8121/aae1d2.